Revealing Band-Hybrid Cooper Pairs on the Surface of a Superconductor with Spin-Orbit Coupling

Javier Zaldívar,[1,*] Jon Ortuzar,[1,*] Miguel Alvarado,[2,3] Stefano Trivini,[1] Julie Baumard,[4]
Carmen Rubio-Verdú,[5] Edwin Herrera,[6] Hermann Suderow,[6] Alfredo Levy Yeyati,[3]
F. Sebastian Bergeret,[4,7] and Jose Ignacio Pascual[1,8,‡]
[1]*CIC nanoGUNE-BRTA, 20018 Donostia-San Sebastián, Spain*
[2]*Instituto de Ciencia de Materiales de Madrid (ICMM), Sor Juana Inés de la Cruz 3, 28049 Madrid, Spain*
[3]*Departamento de Física Teórica de la Materia Condensada, Instituto Nicolás Cabrera and Condensed Matter Physics Center (IFIMAC), Universidad Autónoma de Madrid, Madrid 28049, Spain*
[4]*Centro de Física de Materiales (CFM-MPC), Centro Mixto CSIC-UPV/EHU, 20018 San Sebastián, Spain*
[5]*ICFO, 08860 Castelldefels, Barcelona, Spain*
[6]*Departamento de Física de la Materia Condensada, Instituto Nicolás Cabrera and Condensed Matter Physics Center (IFIMAC), Universidad Autónoma de Madrid, Madrid, Spain*
[7]*Donostia International Physics Center (DIPC), 20018 Donostia-San Sebastián, Spain*
[8]*Ikerbasque, Basque Foundation for Science, Bilbao 48009, Spain*

(Received 6 February 2025; accepted 18 August 2025; published 23 September 2025)

Most superconductors exhibit spin-singlet pairing within a single band. In multiband systems with strong spin-orbit coupling, more exotic scenarios can emerge, including Cooper pairs between bands with distinct symmetries. Here, we present evidence of the formation of Cooper pairs between spin-nondegenerate helical surface bands in the superconductor β-Bi$_2$Pd. Scanning tunneling microscopy reveals anisotropic Yu-Shiba-Rusinov (YSR) resonances induced by vanadium impurities, with long-range amplitude modulations attributed to spin-conserving Bogoliubov quasiparticle interference (BQPI). Analysis of BQPI at the subgap YSR energy shows that only a selective subset of normal-state scattering processes contributes to Cooper pair formation, indicating interband mixing. We trace this selectivity to the hybridization of a helical surface band with others via the impurity.

DOI: 10.1103/6jfy-cv89

The complex formation of Cooper pairs in superconductors underpins many novel states of matter with exotic properties. Because of the antisymmetric nature of the global wave function for two interacting fermions, the orbital character of the electronic bands determines the spin properties of the Cooper pair condensate. As a consequence, pairs in the s-wave (p-wave) channel form a singlet (triplet) state [1], leading to even-in-frequency superconductivity. The presence of spin-orbit coupling (SOC) adds further complexity to the pair formation by lifting spin degeneracies at the superconductor's surface and inducing helical-like bands. As illustrated in Fig. 1, electron pairing within spin-nondegenerate helical bands results in a mixture of spin-singlet and spin-triplet components in the superconducting condensate [2,3], which is essential for the emergence of topological superconductivity [4].

Multiband superconductors broaden the landscape of possible Cooper pair formation in the superconducting condensate [5]. In such a scenario of helical bands as depicted in Fig. 1, electrons from different bands can pair and form hybrid states with finite momentum [6] states or lift the even symmetry or the condensed wave function, enabling odd symmetry pairing schemes [1].

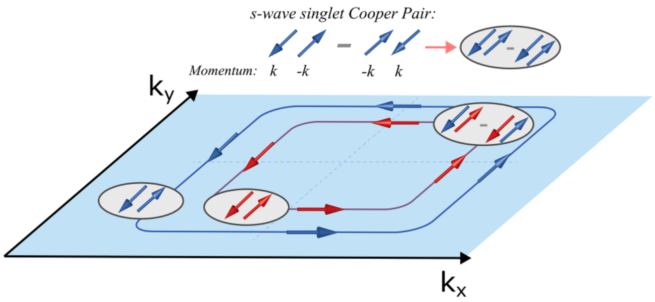

FIG. 1. Illustration of superconducting pairing in a two-helical-band superconductor with the same helicity reported here. Singlet Cooper pair wave function (upper) is formed by electrons in opposite positions in the band (k and $-k$). In the spin-nondegenerate helical bands shown here, only pairs of electrons with locked spin momentum can occur, accounting for mixed singlet and triplet components (intraband Cooper pairs in the sketch). Band hybridization also allows pairing between electrons from different bands, resulting in singlet Cooper pairs of electrons with finite total momentum, overall with zero center of mass momentum.

---

[*] These authors contributed equally to this work.
[†] Contact author: ji.pascual@nanogune.eu

0031-9007/25/135(13)/136201(6)

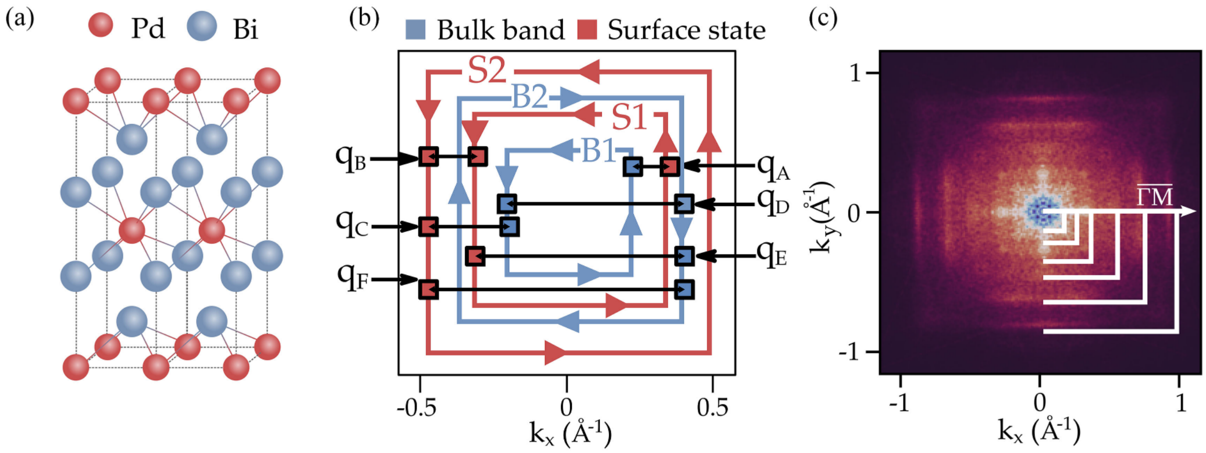

FIG. 2. Quasiparticle interference in -Bi$_2$Pd: (a) Structure of the layered -Bi$_2$Pd superconductor. (b) Schematic band structure on the -Bi$_2$Pd surface, containing two spin-nondegenerate surface bands, $S1$ and $S2$, and two projected bulk bands, $B1$ and $B2$. The blue and red arrows in the contours indicate spin polarization (simplified from Refs. [9,16]). The helical bands $S1$ and $S2$ are spin polarized in plane with the same chirality. The branches with opposite chirality of the Rashba-split bands do not lie on the projected gap [9] and, hence, are not shown here [9]. The vectors q_i represent all possible spin-conserving scattering processes. (c) Fourier transformed dI dV map measured with STM at 50 mV (details in Note II in Supplemental Material [18]) illustrating six contours (solid white lines) representing the six possible QPI scattering vectors between the four bands.

However, despite theoretical predictions, the observation of band-mixed pairing schemes remains challenging because their different orbital character also hinders band hybridization [7,8].

In this Letter, we present evidence of interband pair formation in the surface of the conventional multiband superconductor -Bi$_2$Pd by analyzing subgap Bogoliubov quasiparticle interference (BQPI) patterns arising from magnetic impurities (vanadium adatoms). Using low-temperature scanning tunneling microscopy (STM), we investigate the spatial distribution of Yu-Shiba-Rusinov (YSR) states generated by the V adatoms adsorbed on the Bi-terminated surface. The YSR states display wave-like modulations along the high-symmetry directions of the substrate, characterized by two distinct wavelengths that reveal information about the subgap scattering of Bogoliubov quasiparticles. The band structure on the surface of -Bi$_2$Pd near the Fermi level is governed by two helical bands with a squarelike Fermi contour (as in Fig. 1), which are spin nondegenerate due to the strong SOC and exhibit different topological properties [9]. Similar to quasiparticle interference (QPI) in the normal state [10 14], spin conservation plays a crucial role in the scattering of Bogoliubov quasiparticles. Consequently, intraband BQPI patterns are suppressed for helical bands, allowing for the selective identification of interband scattering processes. Our results agree with the helical nature of these surface proximitized bands and reveal the formation of interband-hybrid Cooper pairs in -Bi$_2$Pd.

-Bi$_2$Pd is a layered material [Fig. 2(a)] with a superconducting transition temperature T_c 5.4 K and strong SOC [15]. Despite its complex band structure around the Fermi level, composed of several bulk bands and surface states with a squarelike Fermi contours [9], -Bi$_2$Pd has a single superconducting gap of .775 meV [16,17]. Owing to the strong SOC, electronic bands at the surface exhibit in-plane spin polarization. Angle-resolved photoemission spectroscopy measurements and density functional theory (DFT) simulations in Refs. [9,16] have found that the -Bi$_2$Pd surface hosts two helical surface bands, $S1$ and $S2$ in Fig. 2(b), spin polarized with the same chirality but with different topological character. The other Rashba components of the two surface states hybridize with bulk bands, vanishing from the projected gaps. The surface of -Bi$_2$Pd also has projected components from several bulk bands, among which two of them, labeled $B1$ and $B2$ in Fig. 2(b), provide significant (spin-polarized) density of states (DOS) at the surface.

Using a low-temperature STM, we measured the normal-state QPI patterns of the as-cleaved Bi-terminated -Bi$_2$Pd surface, mapping the differential conductance (dI dV) at constant sample bias values well above the superconducting gap (see Sec. I in Supplemental Material [18]). The fast Fourier transformation (FFT) of these dI dV maps reveals six squared contours [Fig. 2(c)], indicating the presence of up to six scattering vectors $_i$ in agreement with Refs. [9,16] (Supplemental Material, Sec. II [18]). As depicted in Fig. 2(b), these six vectors and their two-dimensional (2D) contours represent all spin-conserving scattering events between four bands crossing E_F: the surface bands $S1$ and $S2$ and the projected bulk bands $B1$ and $B2$ [25]. We observe no scattering within the same band. As shown in previous studies [10 12] and discussed in more detail in Supplemental Material, Sec. V [18], intraband scattering is forbidden by spin conservation, preventing measurable real-space DOS oscillations.

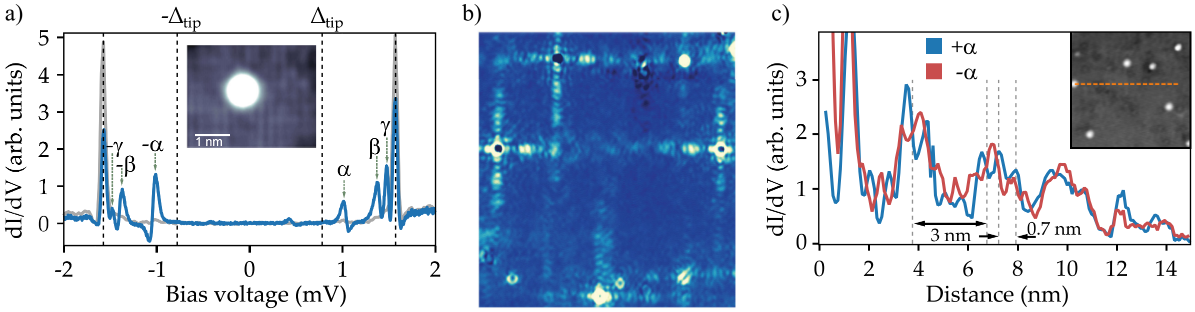

FIG. 3. Anisotropic YSR oscillations: (a) Spectrum on top of the V adatom (blue) shown in the topographic image in the inset. The adatom is 120 pm high. The gray curve is the spectrum of the bare -Bi$_2$Pd surface. The dashed lines mark the superconducting gap of the tip, equal to the -Bi$_2$Pd gap. Set point: V 3 mV, I 3 pA, V_{rms} 25 μV). (b) Intragap dI dV maps at the bias of the α_+ peak (V 1 mV). The white (blue) colors represent the maximum (minimum) dY dV signal. The YSR amplitude is focused in extended beams along the (100) and (010) directions, in agreement with the nesting vectors of the surface bands. The subgap dI dV image was measured along a previously recorded tip profile with set point V 3 mV, I 6 pA. V_{rms} 5 μV; image size: 3 × 3 nm. (c) Distance dependence of the particle (α_+, red) and hole (α , blue) YSR excitation s amplitude along the line in the (100) direction, shown in the topographic inset figure. The quasiparticle interference pattern shows two oscillations, agreeing with the presence of multiple bands. At larger distances from the impurity, the influence of other impurities may affect the pattern. The BQPI patterns of all YSR peaks are shown in Supplemental Material, Fig. S51 [18].

The complex quasiparticle scattering in the normal state anticipates striking effects in the superconducting state, i.e., at subgap energies. To study these, we deposited vanadium atoms on the cold -Bi$_2$Pd substrate [inset of Fig. 3(a)]. The V adatoms act as a spin-dependent scattering potential for Bogoliubov quasiparticles (BQPs), resulting in YSR bound states [26 28]. YSR states are localized around the impurity and are measured as subgap excitations by tunneling electrons or holes, appearing in tunneling spectra as pairs of narrow peaks inside the superconducting gap [29,30]. High-resolution dI dV spectra measured over the V adatoms using a -Bi$_2$Pd-coated tip [31,32] for enhancing the energy resolution [33 36] shows three pairs of YSR peaks, labeled $\alpha_\pm$, $_\pm$, and $\gamma_\pm$ in Fig. 3(a). The peaks correspond to the particle (and hole, at negative bias) excitation of three YSR states formed by the interaction of three spin-polarized d orbitals of V with the -Bi$_2$Pd substrate. As shown in Fig. S4 in [18], the distribution of the YSR signal over the V adatoms follows a pattern of lobes and nodal planes that resembles the amplitude of three different 3d orbitals, in accordance with the survival of a 3d_3 valence state of V on the surface [37,38].

Anisotropic spatial extension of YSR states The subgap YSR states are not simply localized around the impurity, but their amplitude extends for more than 14 nm away from the impurity with a characteristic crosslike tail along the (100) and (010) directions of the substrate [Fig. 3(b)]. The length of these YSR tails is comparable to the coherence length of -Bi$_2$Pd ($\xi_{ab} \sim 23$ nm [15,17,39 41]). Since each YSR state corresponds to the hybridization of an atomic orbital with one of the surface bands [37,38], the long-range oscillatory pattern seen for the α YSR state in Fig. 3(b) entails information about the band hybridized with the impurity and its Fermi contour [42]. The extension of BQPI patterns increases for low-dimensional bands [43,44], but also can be extended by focusing BQPs along one direction, an effect occurring for Fermi band contours with flat portions [37,42,45]. This is the case in -Bi$_2$Pd, where all bands around E_F are quasi-two-dimensional and square shaped [9], with abundant nesting vectors that focus the BQPI scattering along the high-symmetry directions of the surface. This explains the YSR cross-shaped patterns seen in the experimental dI dV images [Fig. 3(b)] and the long, quasi-1D decay of the YSR state [42,45].

Two spatial modulations A closer look at the YSR beams shows that their amplitude spatially oscillates with two different wavelengths, amounting to $\lambda_1 \sim$ .7 and $\lambda_2 \sim 3$ nm. The three YSR states, α, , and γ, show similar long-range patterns for both particle- and holelike excitations (Supplemental Material, Fig. S51 [18]). Figure 3(c) compares particle and hole components of the $\pm\alpha$ YSR state. The shortest oscillation shows a finite particle (p) and hole (h) components dephasing. For the longest oscillation, the p h dephasing is negligible. The dephasing arises from a finite scalar scattering potential in the impurity; see Supplemental Material, Eq. (1) [18]. The different dephasings can be due to a distinct scattering potential for each band.

To identify the bands involved in the YSR oscillations, we increased the coverage of V adatoms and mapped the resulting dense network of YSR oscillations for its FFT analysis. Figure 4(b) presents an intragap dI dV map of an 8 × 8 nm region of -Bi$_2$Pd with 1 V atom coverage, corresponding to the topographic image in Fig. 4(a). Despite the relatively low coverage, YSR resonances from the α_+ state extend from the adatoms, covering approximately 50 of the sample surface. The FFT analysis of the dI dV map in Fig. 4(b) reveals two square contours representing the distribution of BQP scattering vectors $_i$ in the α state [Fig. 4(c)]. From these contours, we

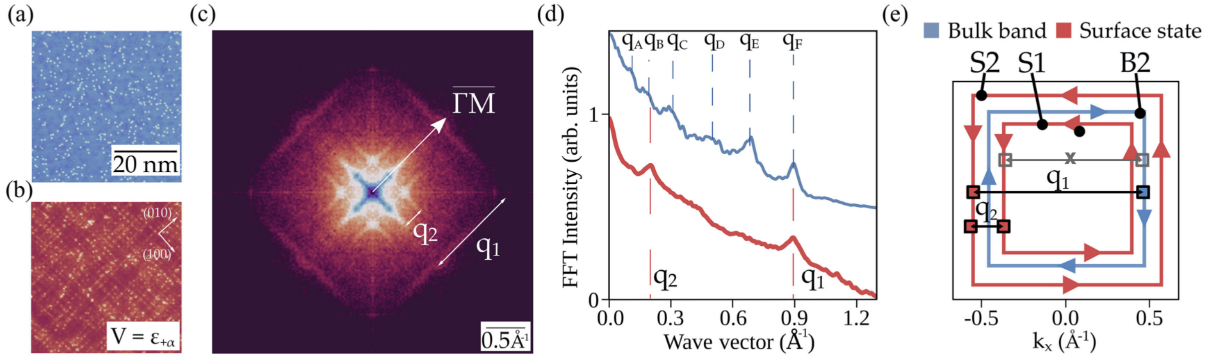

FIG. 4. Fourier transform of Bogoliubov quasiparticle interference: (a) Constant current image (set point: I 1 pA, V 5 mV) and (b) dI dV map of the -Bi$_2$Pd substrate at the energy of the α state (V 1 mV) with 1 coverage of V adatoms. (c) Two-dimensional fast Fourier transform (2DFFT) of the image of (b). The 2DFFT image shows only two contours, in contrast with the 2DFFT of the same sample at energies outside the superconducting gap shown in Fig. 2(c). (d) Comparison of a FFT amplitude along the $\overline{\Gamma M}$ direction between the normal state [blue line, see Fig. 2(c)] and in-gap energy [red line, see white arrow in (c)]. The FFT intensity is averaged over a small area around $\overline{\Gamma M}$. (e) Schematic band s contours from Refs. [9,16], with spin helicity and allowed scattering vectors between the three bands participating in BQPI.

determine scattering vectors $_1$ 2.2 and $_2$ 8.9 nm^{1} [Fig. 4(d)], which correspond to real-space dI dV modulations of 3.1 and 0.7 nm, respectively [Fig. 3(c)].

While the shape of the FFT contours is consistent with the squared symmetry of the -Bi$_2$Pd surface electronic bands [42], the detection of only two square features contrasts with the six scattering contours observed for normal-state QPI in Fig. 2(c). In Fig. 4(d), we compare the FFT intensity along the k_x or $\overline{\Gamma M}$ direction of the BQPI patterns with similar cuts in the (normal state) QPI-FFT map of Fig. 2(c) (see Supplemental Material, Sec. II [18]). The two BQPI vectors $_1$ and $_2$ coincide with $_F$ and $_B$ of the (normal-state) QPI pattern, respectively, while all the other scattering vectors in the normal case are missing in the YSR map. The scattering vectors $_B$ and $_F$ connect the outer surface band $S2$ with the edge of the projected bulk band (with opposite spin helicity) and with the surface band $S1$ (same spin helicity), respectively, as shown in Fig. 2(b). Therefore, these three bands necessarily are involved in the YSR state. Note that, although measured at different energies, the QPI and BQPI can be compared. The bands responsible for the scattering patterns are dispersive, but their relative position (related to the QPI length) are fairly constant, as pointed out in Refs. [9,16].

Band hybridization Model calculations presented in Supplemental Material, Sec. V [18] demonstrate that band hybridization is essential to explain the observed BQPI patterns. For a superconducting system with a magnetic impurity coupled to one of two independent helical bands [straight bands in Fig. 5(a)], the DOS decays smoothly with distance [blue line in Fig. 5(b)]. The absence of oscillations indicates that both intra- and interband BQPI are forbidden, as they involve either different spin states or orthogonal bands. Thus, the lack of oscillations associated with intraband scattering in the experiment agrees with the helical-like polarization of the band structure around E_F. At the same time, we conclude that the observation of two-component YSR oscillations with interband scattering vectors necessarily implies that the participating bands are hybridized.

To account for hybridization between bands, we inserted interband hopping elements in the model of Supplemental Material, Sec. V [18], which coupled the two bands, as shown in Fig. 5(a). The newly formed hybrid bands now allow for the emergence of BQPI oscillations in the DOS [Fig. 5(b)]. Consequently, band hybridization is crucial for

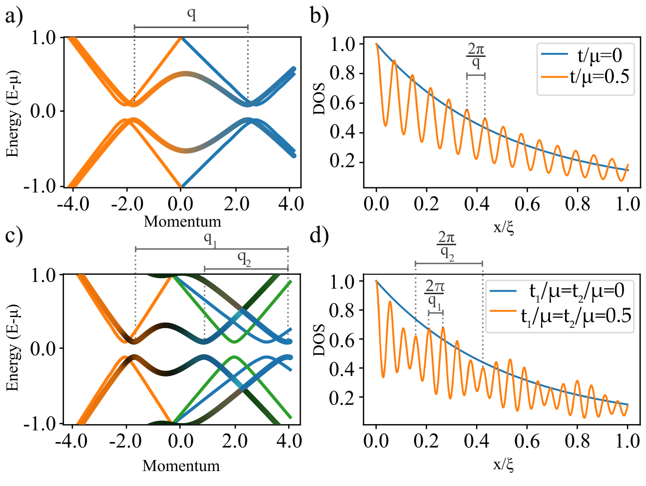

FIG. 5. Theoretical calculations: (a),(c) 1D band structure for a two-band (three-band) model. We plot the original bands (thin lines) and the hybridized ones (thick lines). (b),(d) Decay of the DOS at the YSR energy for the two-band (three-band) model without (blue) and with (orange) interband hopping. The position is normalized by the coherence length ξ. The vectors corresponding to the observed oscillations are marked as q_1 and q_2. t_1 and t_2 refer to the hopping between first and second, and first and third bands, respectively.

generating BQPI (as well as in normal-state QPI) from a single impurity in a system with orthogonal helical bands. It is worth noting that the strong band mixing in the superconducting state of -Bi_2Pd is fully consistent with its single-gap superconductivity. Furthermore, this behavior can be attributed to the significant band overlap in momentum space, as revealed by DFT calculations [9,16].

Intriguingly, the BQPI pattern exhibits only two scattering vectors, $_1$ $_F$ and $_2$ $_B$, connecting the outer band $S2$ with bands $S1$ and $B2$ [Fig. 4(e)], while the third expected vector $_E$ connecting $S1$ with $B2$ is absent. This selectivity arises because YSR excitations, being subgap states, are restricted to bands hybridized with the magnetic impurity. The predominant role of $S2$ in the BQPI patterns indicates that this band forms the YSR channel through its hybridization with the vanadium d orbitals. Consequently, only hybrid pairs with spectral weight in $S2$ contribute to the BQPI at subgap energies, while other hybrid pairs, such as those mixing bands $S1$ and $B2$ (connected through $_E$), do not couple with the impurity, and their quasiparticle excitation energy remains outside the bulk gap.

To demonstrate such selective band interference, we simulate in Fig. 5(c) the DOS of three helical bands, with only one of them coupled to a magnetic impurity. In the absence of interband hopping, the DOS decays smoothly away from the impurity without oscillations [blue line in Fig. 5(d)]. Mixing all the bands with interband hopping elements leads to a single hybrid band with three identical gaps, from which scattering vectors can be obtained. In real space, this configuration results in a two-component BQPI pattern similar to the one we observe in the experiment [orange line in Fig. 5(d)]. Thus, the experimental patterns reflect band mixing effects in the superconducting condensate through the interference pattern of their fermionic excitations.

Above the superconducting gap, all bands are degenerate, and their quasiparticles are sensitive to potential scattering by defects or impurities. In this scenario, all spin-conserving QPI emerges either because interband hopping mixes all bands or, simply, by multi-impurity scattering (both mechanisms are effectively similar, as shown in Supplemental Material, Sec. VI [18]). While SOC could also intrinsically couple the bands, the observation of only spin-conserving wave vectors suggests that a hopping term is a more realistic mechanism to hybridize the selected initial band structure.

Discussion—The multifrequency interference patterns of -Bi_2Pd provide interesting information on pairing mechanisms in this material. First, the lack of BQPI patterns associated with $S2$ intraband scattering corroborates its predicted helical nature. Consequently, the formation of Cooper pairs within this band involves a mixture of singlet and triplet components because an intraband singlet cannot be formed (as depicted in Fig. 1). Furthermore, exotic symmetries in the BCS condensate such as triplet or odd frequency are expected from the hybridization of spin-helical bands with different orbital symmetries [1,46 48].

Since the mixed bands also have different wave vectors, the hybrid Cooper pairs should have a finite momentum. This case resembles the Fulde-Ferrell-Larkin-Ovchinnikov states [49,50], but produced with helical states instead of the Zeeman-split Fermi surface [6]. In this case, the momentum of the BCS condensate averages to zero, but an in-plane magnetic field can induce a net Cooper pair momentum, leading to nonreciprocal currents [51,52] in the surface of the material. Although experimental signatures of such a nontrivial formation of the BCS condensate are not directly evident from the BQPI patterns, our measurements reveal key ingredients for detecting their existence. We foresee that these kinds of BQPI studies, in combination with in-plane magnetic fields [53], could provide further evidence of exotic pairing schemes enabled by multiband coupling.

Acknowledgments—We acknowledge financial support from the Spanish MCIN/AEI/10.13039/501100011033 and the European Regional Development Fund (ERDF) through Grants No. PID2020-114071RB-I00, No. PID2020 114252 GB-I00, No. PID2022-140845OB-C61, No. PID2023-148225NB-C31, No. PID2023-150148OB-I00, No. CEX2020-001038-M, No. CEX2023-001316-M, No. TED2021-130292B-C41, and No. TED2021-130546B-I00, from the Basque Government through Grant No. IT-1591-22, from the European Union NextGenerationEU/PRTR-C17.I1 through the IKUR Strategy of the Department of Education of the Basque Government under a collaboration agreement with Ikerbasque MPC, CIC nanoGUNE, and DIPC, and from the European Union s Horizon Europe through Grant JOSEPHINE (No. 101130224) and through ERC-AdG CONSPIRA (No. 101097693). H. S. and E. H. acknowledge the QUASURF project (ref. SI4/PJI/2024-00199) funded by the Comunidad de Madrid through the agreement to promote and encourage research and technology transfer at the Universidad Autónoma de Madrid. We also acknowledge collaborations through EU program Cost CA21144 (Superqumap). J. O. acknowledges the scholarship PRE-2021-1-0350 from the Basque Government.

Data availability—The data that support the findings of this article are openly available [54].

[1] A. M. Black-Schaffer and A. V. Balatsky, Phys. Rev. B **88**, 104514 (2013).

[2] L. P. Gor kov and E. I. Rashba, Phys. Rev. Lett. **87**, 037004 (2001).

[3] Y. Kim, J. Zhang, E. Rossi, and R. M. Lutchyn, Phys. Rev. Lett. **114**, 236804 (2015).

[4] M. Sato and Y. Ando, Rep. Prog. Phys. **80**, 076501 (2017).

[5] Y. Asano and A. Sasaki, Phys. Rev. B **92**, 224508 (2015).

[6] T. Asaba, M. Naritsuka, H. Asaeda, Y. Kosuge, S. Ikemori, S. Suetsugu, Y. Kasahara, Y. Kohsaka, T. Terashima, A. Daido, Y. Yanase, and Y. Matsuda, Nat. Commun. **15**, 3861 (2024).

[7] P. O. Sprau, A. Kostin, A. Kreisel, A. E. Böhmer, V. Taufour, P. C. Canfield, S. Mukherjee, P. J. Hirschfeld, B. M. Andersen, and J. C. Davis, Science **357**, 75 (2017).

[8] R. Sharma, S. D. Edkins, Z. Wang, A. Kostin, C. Sow, Y. Maeno, A. P. Mackenzie, J. C. Séamus Davis, and V. Madhavan, Proc. Natl. Acad. Sci. U.S.A. **117**, 5222 (2020).

[9] M. Sakano, K. Okawa, M. Kanou, H. Sanjo, T. Okuda, T. Sasagawa, and K. Ishizaka, Nat. Commun. **6**, 8595 (2015).

[10] L. Petersen and P. Hedegård, Surf. Sci. **459**, 49 (2000).

[11] J. I. Pascual, G. Bihlmayer, Yu. M. Koroteev, H.-P. Rust, G. Ceballos, M. Hansmann, K. Horn, E. V. Chulkov, S. Blügel, P. M. Echenique, and Ph. Hofmann, Phys. Rev. Lett. **93**, 196802 (2004).

[12] A. Stró ecka, A. Eiguren, and J. I. Pascual, Phys. Rev. Lett. **107**, 186805 (2011).

[13] M. Steinbrecher, H. Harutyunyan, C. R. Ast, and D. Wegner, Phys. Rev. B **87**, 245436 (2013).

[14] E. Herrera, I. Guillamón, V. Barrena, W. J. Herrera, J. A. Galvis, A. L. Yeyati, J. Rusz, P. M. Oppeneer, G. Knebel, J. P. Brison, J. Flouquet, D. Aoki, and H. Suderow, Nature (London) **616**, 465 (2023).

[15] Y. Imai, F. Nabeshima, T. Yoshinaka, K. Miyatani, R. Kondo, S. Komiya, I. Tsukada, and A. Maeda, J. Phys. Soc. Jpn. **81**, 113708 (2012).

[16] K. Iwaya, Y. Kohsaka, K. Okawa, T. Machida, M. S. Bahramy, T. Hanaguri, and T. Sasagawa, Nat. Commun. **8**, 976 (2017).

[17] E. Herrera, I. Guillamón, J. A. Galvis, A. Correa, A. Fente, R. F. Luccas, F. J. Mompean, M. García-Hernández, S. Vieira, J. P. Brison, and H. Suderow, Phys. Rev. B **92**, 054507 (2015).

[18] See Supplemental Material at http://link.aps.org/supplemental/10.1103/6jfy-cv89 which also includes Refs. [19 24], for additional experimental results and details of the theoretical model.

[19] Q.-H. Wang and D.-H. Lee, Phys. Rev. B **67**, 020511(R) (2003).

[20] C. Bena and S. A. Kivelson, Phys. Rev. B **72**, 125432 (2005).

[21] A. V. Balatsky, I. Vekhter, and J.-X. Zhu, Rev. Mod. Phys. **78**, 373 (2006).

[22] Y. Kohsaka, T. Machida, K. Iwaya, M. Kanou, T. Hanaguri, and T. Sasagawa, Phys. Rev. B **95**, 115307 (2017).

[23] A. Dutt, A. A. Golubov, O. V. Dolgov, and D. V. Efremov, Phys. Rev. B **96**, 054513 (2017).

[24] M. M. Korshunov, Y. N. Togushova, and O. V. Dolgov, Phys. Usp. **59**, 1211 (2016).

[25] J. I. Pascual, A. Dick, M. Hansmann, H.-P. Rust, J. Neugebauer, and K. Horn, Phys. Rev. Lett. **96**, 046801 (2006).

[26] L. Yu, Acta Phys. Sin. **21**, 75 (1965).

[27] H. Shiba, Prog. Theor. Phys. **40**, 435 (1968).

[28] A. I. Rusinov, Sov. J. Exp. Theor. Phys. **29**, 1101 (1969).http://jetp.ras.ru/cgi-bin/e/index/e/29/6/p1101?a=list

[29] S.-H. Ji, T. Zhang, Y.-S. Fu, X. Chen, X.-C. Ma, J. Li, W.-H. Duan, J.-F. Jia, and Q.-K. Xue, Phys. Rev. Lett. **100**, 226801 (2008).

[30] B. W. Heinrich, J. I. Pascual, and K. J. Franke, Prog. Surf. Sci. **93**, 1 (2018).

[31] D. J. Choi, C. G. Fernández, E. Herrera, C. Rubio-Verdú, M. M. Ugeda, I. Guillamón, H. Suderow, J. I. Pascual, and N. Lorente, Phys. Rev. Lett. **120**, 167001 (2018).

[32] S. Trivini, J. Ortuzar, J. Zaldivar, E. Herrera, I. Guillamón, H. Suderow, F. S. Bergeret, and J. I. Pascual, Phys. Rev. B **110**, 235405 (2024).

[33] S. H. Pan, E. W. Hudson, and J. C. Davis, Appl. Phys. Lett. **73**, 2992 (1998).

[34] H. Suderow, M. Crespo, P. Martinez-Samper, J. G. Rodrigo, G. Rubio-Bollinger, S. Vieira, N. Luchier, J. P. Brison, and P. C. Canfield, Physica (Amsterdam) **369C**, 106 (2002).

[35] J. G. Rodrigo, H. Suderow, and S. Vieira, Eur. Phys. J. B **40**, 483 (2004).

[36] K. J. Franke, G. Schulze, and J. I. Pascual, Science **332**, 940 (2011).

[37] M. Ruby, Y. Peng, F. von Oppen, B. W. Heinrich, and K. J. Franke, Phys. Rev. Lett. **117**, 186801 (2016).

[38] D.-J. Choi, C. Rubio-Verdú, J. de Bruijckere, M. M. Ugeda, N. Lorente, and J. I. Pascual, Nat. Commun. **8**, 15175 (2017).

[39] J. Kačmarčík, Z. Pribulová, T. Samuely, P. Szabó, V. Cambel, J. oltýs, E. Herrera, H. Suderow, A. Correa-Orellana, D. Prabhakaran, and P. Samuely, Phys. Rev. B **93**, 144502 (2016).

[40] G. Pristáš, M. Orendáč, S. Gabáni, J. Kačmarčík, E. Gažo, Z. Pribulová, A. Correa-Orellana, E. Herrera, H. Suderow, and P. Samuely, Phys. Rev. B **97**, 134505 (2018).

[41] L. Che, T. Le, C. Q. Xu, X. Z. Xing, Z. Shi, X. Xu, and X. Lu, Phys. Rev. B **94**, 024519 (2016).

[42] J. Ortuzar, S. Trivini, M. Alvarado, M. Rouco, J. Zaldivar, A. L. Yeyati, J. I. Pascual, and F. S. Bergeret, Phys. Rev. B **105**, 245403 (2022).

[43] G. C. Ménard, S. Guissart, C. Brun, S. Pons, V. S. Stolyarov, F. Debontridder, M. V. Leclerc, E. Janod, L. Cario, D. Roditchev, P. Simon, and T. Cren, Nat. Phys. **11**, 1013 (2015).

[44] H. Kim, L. Rózsa, D. Schreyer, E. Simon, and R. Wiesendanger, Nat. Commun. **11**, 4573 (2020).

[45] M. Uldemolins, A. Mesaros, and P. Simon, Phys. Rev. B **105**, 144503 (2022).

[46] F. S. Bergeret, A. F. Volkov, and K. B. Efetov, Rev. Mod. Phys. **77**, 1321 (2005).

[47] F. S. Bergeret and A. F. Volkov, Ann. Phys. (N.Y.) **456**, 169232 (2023).

[48] S. Kanasugi and Y. Yanase, Commun. Phys. **5**, 39 (2022).

[49] P. Fulde and R. A. Ferrell, Phys. Rev. **135**, A550 (1964).

[50] A. I. Larkin, and Yu. N. Ovchinnikov, Sov. Phys. JETP **20**, 762 (1965).

[51] N. F. Q. Yuan and L. Fu, Proc. Natl. Acad. Sci. U.S.A. **119**, e2119548119 (2022).

[52] S. Ilić and F. S. Bergeret, Phys. Rev. Lett. **128**, 177001 (2022).

[53] L. Powell, W. Kuang, G. Hawkins-Pottier, R. Jalil, J. Birkbeck, Z. Jiang, M. Kim, Y. Zou, S. Komrakova, S. Haigh, I. Timokhin, G. Balakrishnan, A. K. Geim, N. Walet, A. Principi, and I. V. Grigorieva, Nat. Commun. **16**, 291 (2025).

[54] J. Zaldívar, J. Ortuzar, M. Alvarado, S. Trivini, J. Baumard, C. Rubio-Verdú, E. Herrera, H. Suderow, A. Levy Yeyati, F. S. Bergeret, and J. I. Pascual, Dataset for Revealing band-hybrid Cooper pairs on the surface of a superconductor with spin-orbit coupling, Zenodo, 2025, 10.5281/zenodo.16925543.